Mon. Not. R. Astron. Soc. **365,** 1021–1030 (2006) doi:10.1111/j.1365-2966.2005.09788.x

The baryon fraction in hydrodynamical simulations of galaxy clusters

S. Ettori,[1⋆] K. Dolag,[2⋆] S. Borgani[3,4,5⋆] and G. Murante[6⋆]

[1]*INAF, Osservatorio Astronomico di Bologna, via Ranzani 1, I-40127 Bologna, Italy*
[2]*Max-Planck-Institut für Astrophysik, Karl-Schwarzschild Strasse 1, Garching bei München, Germany*
[3]*Dipartimento di Astronomia dell'Università di Trieste, via Tiepolo 11, I-34131 Trieste, Italy*
[4]*INFN – National Institute for Nuclear Physics, Trieste, Italy*
[5]*CISC – Interdepartmental Centre for Computational Sciences, University of Trieste, Italy*
[6]*INAF, Osservatorio Astronomico di Torino, Strada Osservatorio 20, I-10025 Pino Torinese, Italy*

Accepted 2005 October 25. Received 2005 October 1; in original form 2005 June 20

ABSTRACT

We study the baryon mass fraction in a set of hydrodynamical simulations of galaxy clusters performed using the Tree+SPH code GADGET-2. We investigate the dependence of the baryon fraction upon radiative cooling, star formation, feedback through galactic winds, conduction and redshift. Both the cold stellar component and the hot X-ray-emitting gas have narrow distributions that, at large cluster-centric distances $r \gtrsim R_{500}$, are nearly independent of the physics included in the simulations. Only the non-radiative runs reproduce the gas fraction inferred from observations of the inner regions ($r \approx R_{2500}$) of massive clusters. When cooling is turned on, the excess star formation is mitigated by the action of galactic winds, yet not by the amount required by observational data. The baryon fraction within a fixed overdensity increases slightly with redshift, independent of the physical processes involved in the accumulation of baryons in the cluster potential well. In runs with cooling and feedback, the increase in baryons is associated with a larger stellar mass fraction that arises at high redshift as a consequence of more efficient gas cooling. For the same reason, the gas fraction appears less concentrated at higher redshift. We discuss the possible cosmological implications of our results, and find that two assumptions generally adopted, i.e. (1) mean value of $Y_{\rm b} = f_{\rm b}/(\Omega_{\rm b}/\Omega_{\rm m})$ not evolving with redshift, and (2) a fixed ratio between $f_{\rm star}$ and $f_{\rm gas}$ independent of radius and redshift, might not be valid. In the estimate of the cosmic matter density parameter, this implies some systematic effects of the order of $\Delta\Omega_{\rm m}/\Omega_{\rm m} \lesssim +0.15$ for non-radiative runs and $\Delta\Omega_{\rm m}/\Omega_{\rm m} \approx +0.05$ and $\lesssim -0.05$ for radiative simulations.

Key words: methods: numerical – galaxies: clusters: general – cosmology: miscellaneous – X-rays: galaxies.

1 INTRODUCTION

Baryons in galaxy clusters, mainly in the form of stars in galaxies and hot X-ray-emitting plasma, trace the potential of the collapsed structure into which they fall. At the same time, their spatial distribution and thermodynamical properties are affected by the physical processes acting on them. Measurement of direct cluster observables, such as stellar optical light and hot gas X-ray emission, is the only viable approach to investigate the physics that drives the evolution of such structures. The observed relations among proxies of the internal energy and entropy levels show that, at least in massive systems, the dominant baryonic component of the intracluster medium (ICM) has a luminosity, temperature and mass that well follow those predicted under the assumptions of a plasma emitting by bremsstrahlung and sitting in hydrostatic equilibrium with the underlying dark matter (DM) potential (e.g. Kaiser 1991; Evrard & Henry 1991).

Moreover, the fact that galaxy clusters are relatively well-isolated structures, which form in correspondence to the highest peaks of the primordial gravitational fluctuations, suggests that their relative baryon budget and the mass function are highly sensitive tests of the geometry and matter content of the Universe. In particular, using X-ray observations of the baryonic content to infer the gas and total mass of relaxed clusters in hydrostatic equilibrium allows one to place a lower limit to the cluster baryon mass fraction, which is expected to match the cosmic value $\Omega_{\rm b}/\Omega_{\rm m}$ (White et al. 1993; Evrard 1997; Mohr, Mathiesen & Evrard 1999; Ettori & Fabian 1999; Roussel, Sadat & Blanchard 2000; Allen, Schmidt & Fabian 2002; Ettori, Tozzi & Rosati 2003; Ettori 2003; Allen et al. 2004).

⋆E-mail: stefano.ettori@bo.astro.it (SE); kdolag@mpa-garching.mpg.de (KD); borgani@ts.astro.it (SB); murante@to.astro.it (GM)

The purpose of the present work is to use an extended set of hydrodynamical simulations of galaxy clusters, treating a variety of physical processes, to study how the spatial distribution of the baryons, as contributed both by the stellar component and by the hot X-ray-emitting gas, are affected by the physical conditions within clusters. In this respect, our analysis extends previous analyses of the baryon fraction in cluster simulations, which included only non-radiative physics (Evrard 1990; Metzler & Evrard 1994; Navarro, Frenk & White 1995; Lubin et al. 1996; Eke, Navarro & Frenk 1998; Frenk et al. 1999; Mohr et al. 1999; Bialek, Evrard & Mohr 2001) and the processes of cooling and star formation (Muanwong et al. 2002; Kay et al. 2004; Ettori et al. 2004; Kravtsov, Nagai & Vikhlinin 2005).

The paper is organized as follows. In Section 2, we describe our data set of simulated galaxy clusters. In Section 3, we present the results obtained from this set of simulations on the gas and baryon fraction, also comparing these results to the observational constraints. In Section 4, we compare our results with previous analyses based on different simulations. Finally, we summarize and discuss our findings in Section 5.

2 PROPERTIES OF THE SIMULATED CLUSTERS

We consider two sets of clusters, which have been selected from different parent cosmological boxes. The first set is extracted from the large-scale cosmological simulation presented in Borgani et al. (2004). The second one is a re-simulation of nine galaxy clusters, extracted from a pre-existing lower-resolution DM-only simulation. Our simulations were carried out with GADGET-2 (Springel 2005), a new version of the parallel Tree+SPH simulation code GADGET (Springel, Yoshida & White 2001). It includes an entropy-conserving formulation of smoothed particle hydrodynamics (SPH; Springel & Hernquist 2002), radiative cooling, heating by an ultraviolet (UV) background, and a treatment of star formation and feedback from galactic winds powered by supernova explosions (Springel & Hernquist 2003).

2.1 Clusters extracted from a cosmological box

The first set of simulated clusters has been extracted from the large-scale cosmological simulation of a 'concordance' ΛCDM model ($\Omega_{0\rm m} = 0.3$, $\Omega_{0\Lambda} = 0.7$, $\Omega_{0\rm b} = 0.019\,h^{-2}$, $h = 0.7$, $\sigma_8 = 0.8$; Borgani et al. 2004). Here we give only a short summary of its characteristics, and refer to that paper for more details. The run follows the evolution of 480^3 dark matter particles and an equal number of gas particles in a periodic cube of size $192\,h^{-1}$ Mpc. The mass of the gas particles is $m_{\rm gas} = 6.89 \times 10^8\,h^{-1}\,{\rm M}_\odot$, while the Plummer-equivalent force softening is set to $7.5\,h^{-1}$ kpc from $z = 0$ to $z = 2$, and is kept fixed in comoving units at higher redshift. At $z = 0$ we extract a set of 439 mass-selected clusters with virial masses $M_{\rm vir} > 5 \times 10^{13}\,h^{-1}\,{\rm M}_\odot$.

The efficiency of conversion of the energy provided by supernova (SN) explosions into kinetic feedback (i.e. winds) is set to 50 per cent, which gives a wind speed of $\approx$340 km s^{-1}.

2.2 Re-simulated clusters

This set includes simulations of four high-mass systems with $M_{200} = (1.1\text{–}1.8) \times 10^{15}\,h^{-1}\,{\rm M}_\odot$. The cluster regions were extracted from a 'dark matter only' simulation with a box size of $479\,h^{-1}$ Mpc of the same cosmological model as the first set, but with a higher normalization of the power spectrum, $\sigma_8 = 0.9$ (see Yoshida, Sheth & Diaferio 2001). Using the 'zoomed initial conditions' (ZIC) technique (Tormen 1997), they were re-simulated with higher mass and force resolution by populating their Lagrangian volumes in the initial domain with more particles, while appropriately adding additional high-frequency modes. The initial particle distributions (before displacement) are of glass type (White 1996). The mass resolution of the gas particles in these simulations $m_{\rm gas} = 1.7 \times 10^8\,h^{-1}\,{\rm M}_\odot$. Thus, the clusters were resolved with between 2×10^6 and 4×10^6 particles, depending on their final mass. For all simulations, the gravitational softening length was kept fixed at $\epsilon = 30.0\,h^{-1}$ kpc comoving (Plummer equivalent), and was switched to a physical softening length of $\epsilon = 5.0\,h^{-1}$ kpc at $z = 5$.

For simulations including star formation and feedback, the SN efficiency in powering galactic winds is set to 50 per cent, as in the cosmological box, which turns into a wind speed of $\approx$340 km s^{-1}. For the sake of comparison, some runs have also been performed with the winds switched off completely or with the SN efficiency increased to unity.

For some of the cluster simulations we also included the effect of heat conduction. Its implementation in SPH, which is both stable and manifestly conserves thermal energy even with individual and adaptive time-steps, has been described by Jubelgas, Springel & Dolag (2004). This implementation assumes an isotropic effective conductivity parametrized as a fixed fraction of the Spitzer rate, which we assume to be 1/3. It also accounts for saturation, which can become relevant in low-density gas. For more details on the properties of simulated galaxy clusters, including thermal conduction, see Dolag et al. (2004).

Furthermore, some simulations were carried out using a modified artificial viscosity scheme suggested by Morris & Monaghan (1997), where every particle evolves its own viscosity parameter. Whereas in this scheme shocks are as well captured as in the standard one, regions with no shocks do not suffer from a residual non-vanishing artificial viscosity. Therefore, turbulence driven by fluid instabilities can be much better resolved and, as a result of this, galaxy clusters simulated with this new scheme can build up a sufficient level of turbulence-powered instabilities along the surfaces of the large-scale velocity structure present in cosmological structure formation (Dolag et al. 2005).

In summary, this set of clusters was simulated four times, with different kinds of physical processes included, as follows:

(i) *Gravitational heating only (code = G).*

(ii) *Gravitational heating only with low viscosity (code = GV).* This is like G, but using the alternative implementation of artificial viscosity. In this simulation, galaxy clusters are found to have up to 30 per cent of their thermal energy in the turbulent motion of the ICM, leading to a sizeable contribution of non-thermal pressure support in the centre of galaxy clusters.

(iii) *Cooling plus star formation plus feedback with weak winds* (*code = FwW*). Here the wind speed is fixed at $\approx$340 km s^{-1}.

(iv) *Cooling plus star formation plus feedback with weak winds and conduction* (*code = FwWC*). The conduction efficiency is set to be one-third of the Spitzer rate.

In order to have under control the effect of changing the feedback efficiency, one high-mass cluster was further simulated with the following setups:

(i) *Cooling plus star formation plus feedback with no winds* (*code = F*). This is like FwW, but with winds switched off.

(ii) *Cooling plus star formation plus feedback with strong winds* (*code* = *FsW*). This is like FwW, but with wind speed increased to $\approx$480 km s^{-1}, corresponding to a SN efficiency of unity.

The centre of each cluster is defined as the position of the particle having the minimum value of the gravitational potential. Starting from this position, we run a spherical overdensity algorithm to find the radius R_{Δ_c} encompassing a given overdensity Δ_c, with respect to the critical one at the redshift under examination, and the mass M_{Δ_c} enclosed within this radius. In the present work, we consider values of the overdensity Δ_c equal to 2500, 500 and 200. The corresponding radii relate to the virial radius, which defines a sphere with virial overdensity (of $\approx$101 at $z = 0$ and $\approx$157 at $z = 1$ for our cosmological model and with respect to the critical value), as $(R_{2500}, R_{500}, R_{200}) \approx (0.2, 0.5, 0.7) \times R_{\rm vir}$. For each cluster, the hot gas mass fraction and the stellar mass fraction within a given radius r are then calculated as $f_{\rm gas}(<r) = M_{\rm gas}(<r)/M_{\rm tot}(<r)$ and $f_{\rm star}(<r) = M_{\rm star}(<r)/M_{\rm tot}(<r)$, respectively.

3 RESULTS FOR THE GAS AND STELLAR MASS FRACTIONS

For the sake of clarity, we define the quantities $Y_{\rm gas}$, $Y_{\rm star}$ and $Y_{\rm b}$ to be the ratios of $f_{\rm gas}$, $f_{\rm star}$ and $f_{\rm b} = f_{\rm gas} + f_{\rm star}$ to the cosmic value adopted in the present simulations, $\Omega_{\rm b}/\Omega_{\rm m} = 0.13$. Their mean values (and standard deviations of the observed distributions, where available) at redshift $z = 0$, 0.3, 0.7 and 1 are quoted in Table 1 for the different physical conditions considered.

In Fig. 1 we compare the gas and baryon fractions as a function of the virial mass, both for the simulated clusters extracted from the cosmological box and for the subset of the re-simulated ones with $M_{200} > 10^{15}\,h^{-1}\,{\rm M}_\odot$. This plot demonstrates that, when computed within the whole cluster virial region, there is no relevant dependence upon mass of such fractions. We remind the reader that the two sets of clusters have been simulated for the same cosmological model, the only difference being in the value of σ_8, assumed to be 0.8 and 0.9 for the first and the second set, respectively. In Fig. 1, the re-simulated clusters indicated with a diamond correspond to the same simulation physics as for the clusters extracted from the cosmological box. They show a mean $Y_{\rm b}$ consistent with that measured for the massive systems of the cosmological box, but with a slightly lower value of $Y_{\rm gas}$. This is due to the increase in the cooling efficiency with the amplitude of the power spectrum, which produces more evolved clusters (Borgani et al., in preparation).

The radial distribution of the gas and baryon mass fractions in these massive systems present quite a similar behaviour. For one representative object, in Fig. 2 we plot these ratios as a function of radius, out to 3 R_{200}, at $z = 0$ and 1, for the six physical schemes adopted in our analysis. The total baryon fraction measured in the radiative models is higher than the value obtained for the non-radiative runs (code = G, GV) within the virial radius and reaches the cosmic value at about 3 R_{200}. The gas fraction is larger when the winds are stronger as a consequence of their effect in preventing gas removal from the hot phase. At $z = 0$, it increases typically with radius reaching 50 and 80 per cent of the value measured at R_{200} at $r \lesssim 0.1\,R_{200}$ and at $\sim 0.3\,R_{200}$, respectively. At $z = 1$, the gas fraction is less concentrated: the radii at which 50 and 80 per cent of $f_{\rm gas}(<R_{200})$ is reached are factors of 1.4 and 2 larger than at $z = 0$.

The quantities $Y_{\rm gas}$ and $Y_{\rm b}$ at R_{2500}, R_{500} and R_{200}, as a function of redshift and physics included in the simulations, are plotted in Fig. 3. In the inner cluster regions, the dissipative action of

Table 1. Distribution of the baryons in the two sets of simulated galaxy clusters. The mean values of the indicated ratios are shown.

Status	N	z	R_{2500}			R_{500}			R_{200}		
			$Y_{\rm gas}$	$Y_{\rm star}$	$Y_{\rm b}$	$Y_{\rm gas}$	$Y_{\rm star}$	$Y_{\rm b}$	$Y_{\rm gas}$	$Y_{\rm star}$	$Y_{\rm b}$
G	4	0.0	0.817(0.064)	–	0.817(0.064)	0.874(0.023)	–	0.874(0.023)	0.894(0.020)	–	0.894(0.020)
		0.3	0.864(0.057)	–	0.864(0.057)	0.907(0.022)	–	0.907(0.022)	0.926(0.019)	–	0.926(0.019)
		0.7	0.888(0.020)	–	0.888(0.020)	0.945(0.028)	–	0.945(0.028)	0.933(0.027)	–	0.933(0.027)
		1.0	0.910(0.094)	–	0.910(0.094)	0.947(0.037)	–	0.947(0.037)	0.942(0.033)	–	0.942(0.033)
GV	4	0.0	0.690(0.045)	–	0.690(0.045)	0.818(0.018)	–	0.818(0.018)	0.864(0.010)	–	0.864(0.010)
		0.3	0.720(0.069)	–	0.720(0.069)	0.865(0.019)	–	0.865(0.019)	0.900(0.013)	–	0.900(0.013)
		0.7	0.720(0.033)	–	0.720(0.033)	0.914(0.038)	–	0.914(0.038)	0.913(0.025)	–	0.913(0.025)
		1.0	0.722(0.106)	–	0.722(0.106)	0.912(0.045)	–	0.912(0.045)	0.935(0.016)	–	0.935(0.016)
FwW	4	0.0	0.513(0.021)	0.419(0.029)	0.931(0.021)	0.658(0.029)	0.262(0.011)	0.920(0.026)	0.701(0.027)	0.226(0.009)	0.927(0.018)
		0.3	0.448(0.040)	0.565(0.054)	1.013(0.063)	0.664(0.025)	0.286(0.022)	0.950(0.027)	0.708(0.018)	0.243(0.018)	0.951(0.019)
		0.7	0.341(0.059)	0.749(0.114)	1.090(0.060)	0.649(0.024)	0.305(0.021)	0.953(0.014)	0.687(0.028)	0.259(0.013)	0.946(0.019)
		1.0	0.288(0.036)	0.884(0.098)	1.172(0.090)	0.631(0.036)	0.330(0.038)	0.961(0.028)	0.684(0.029)	0.269(0.019)	0.953(0.033)
FwWC	4	0.0	0.538(0.058)	0.398(0.049)	0.935(0.021)	0.655(0.031)	0.257(0.015)	0.912(0.027)	0.714(0.027)	0.221(0.011)	0.936(0.017)
		0.3	0.448(0.070)	0.552(0.072)	1.000(0.063)	0.652(0.026)	0.281(0.017)	0.932(0.025)	0.726(0.026)	0.236(0.017)	0.962(0.014)
		0.7	0.302(0.090)	0.803(0.169)	1.105(0.079)	0.631(0.028)	0.306(0.018)	0.937(0.017)	0.707(0.034)	0.250(0.008)	0.958(0.027)
		1.0	0.247(0.052)	0.965(0.160)	1.212(0.126)	0.620(0.058)	0.327(0.048)	0.946(0.025)	0.704(0.033)	0.263(0.021)	0.967(0.027)
F	1	0.0	0.294(–)	0.682(–)	0.976(–)	0.535(–)	0.370(–)	0.905(–)	0.593(–)	0.333(–)	0.927(–)
		0.3	0.169(–)	1.083(–)	1.252(–)	0.491(–)	0.447(–)	0.938(–)	0.594(–)	0.369(–)	0.963(–)
		0.7	0.123(–)	1.465(–)	1.588(–)	0.456(–)	0.486(–)	0.942(–)	0.564(–)	0.371(–)	0.935(–)
		1.0	0.180(–)	1.054(–)	1.234(–)	0.558(–)	0.409(–)	0.967(–)	0.578(–)	0.362(–)	0.940(–)
FsW	1	0.0	0.638(–)	0.302(–)	0.939(–)	0.699(–)	0.199(–)	0.898(–)	0.747(–)	0.176(–)	0.923(–)
		0.3	0.600(–)	0.439(–)	1.038(–)	0.731(–)	0.245(–)	0.976(–)	0.774(–)	0.203(–)	0.978(–)
		0.7	0.439(–)	0.617(–)	1.055(–)	0.718(–)	0.263(–)	0.981(–)	0.740(–)	0.210(–)	0.951(–)
		1.0	0.409(–)	0.552(–)	0.960(–)	0.745(–)	0.248(–)	0.993(–)	0.730(–)	0.207(–)	0.937(–)

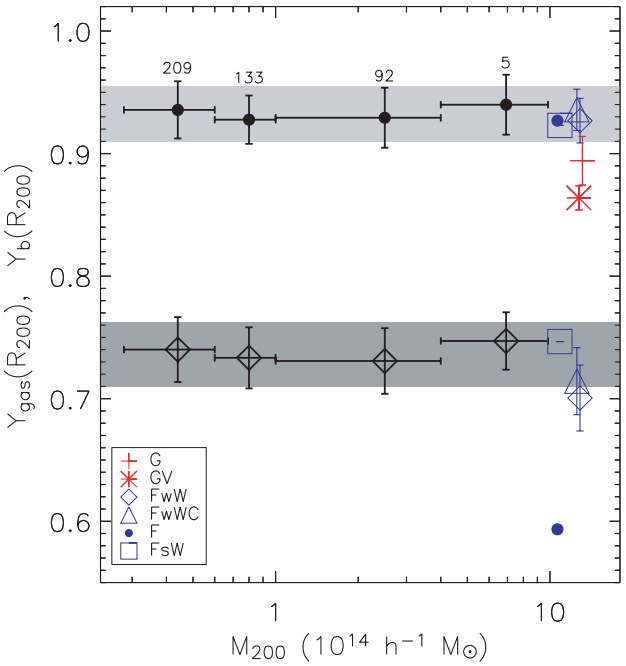

Figure 1. The baryon and gas mass fractions at R_{200} and $z = 0$ as functions of the virial mass. The full circles with error bars refer to the mean and dispersion measured in the corresponding bins in virial mass. The number of objects in each bin is indicated. The most massive re-simulated systems are also shown. The shaded regions indicate the 1σ range of Y_{gas} and Y_b for the set of simulated clusters extracted from the cosmological box.

radiative cooling enhances the average Y_b to supercosmic values at high redshift. At late times, cooling is less efficient, and Y_b declines, although to values ($\sim$0.9 at $z = 0$) that remain higher than those of the non-radiative runs. A smaller scatter and more widespread agreement among the different physical regimes are instead found in the outskirts ($r \gtrsim R_{500}$). The gas fraction within R_{2500} is about 0.3 times the cosmic value at $z = 1$ and 0.6 at $z = 0$, whereas is more tightly distributed around 0.6–0.7 at larger radii, with evidence of larger values in the presence of strong winds. We also compare in Fig. 3 our simulation results with the observed f_{gas} distribution in highly X-ray-luminous clusters at R_{2500} (from Allen et al. 2004) and at R_{500} (from Ettori & Fabian 1999). Simulations clearly indicate a sizeable underestimate of the hot baryon budget, both at R_{2500} and at R_{500}. When extra physics is added to the action of gravitational heating, lower hot gas fractions result. The discrepancy with the inferred observed fraction signals the existence of systematic errors, either in our physical treatment, or in estimates of the observed fraction, or possibly both. It is worth noting that total mass estimates, for instance, suffer from systematic differences when measured from X-ray analysis and from dark matter particles in simulations, mainly owing to bias in the X-ray spectral temperature measurements [see e.g. Mazzotta et al. (2004) and Vikhlinin (2005) and, specifically related to the systematics in X-ray mass estimates, Rasia et al. (2005)]. The observed gas fraction measurements are well represented by the values measured in the non-radiative simulations also in the inner regions, where variations by $\lesssim$15 per cent due to the action of non-thermal pressure support (induced by the reduced viscosity scheme) encompass the observed variance.

The values of, and the relation between, Y_{gas} and Y_{star} are shown in Figs 4 and 5. At R_{2500}, the estimate of Y_b is strongly affected by the physics involved in the accumulation of the cluster baryons, with supercosmic values mainly due to a very high star formation

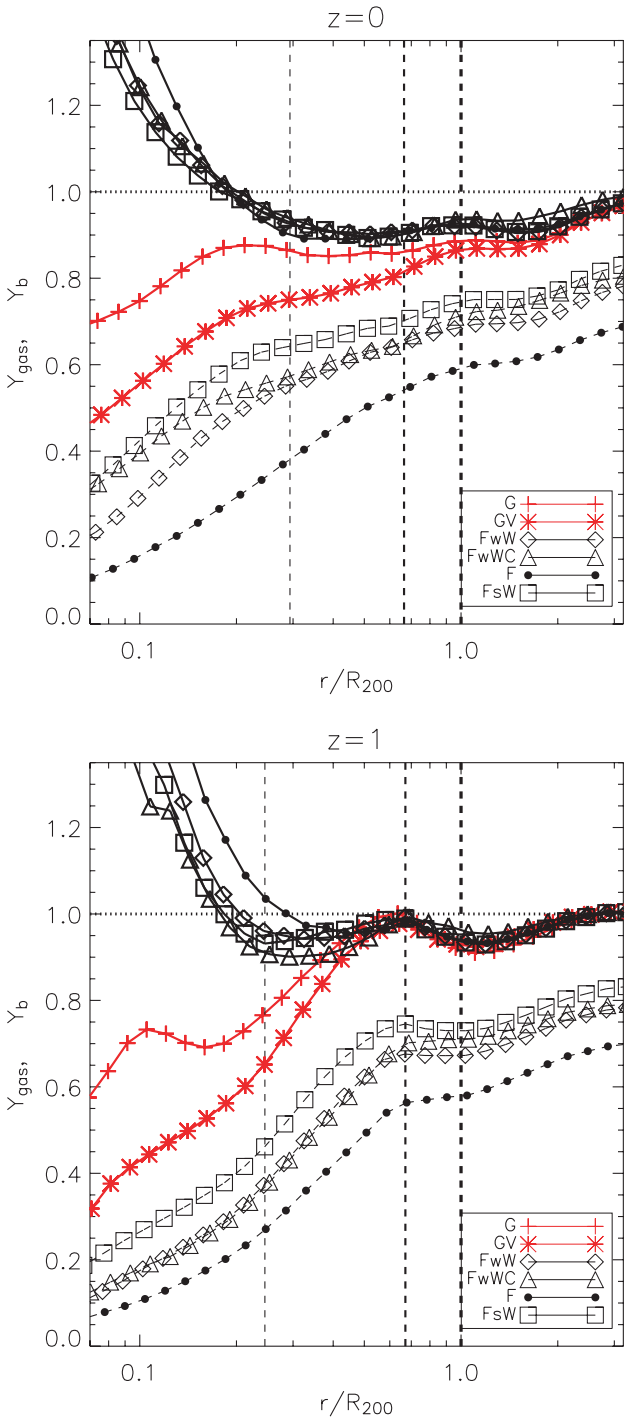

Figure 2. The radial distribution of the gas and baryon mass fractions (in units of the cosmic baryonic value) at $z = 0$ and 1 for one of the four massive re-simulated systems. The vertical dashed lines indicate the location of R_{2500}, R_{500} and R_{200} for the case of gravitational heating only.

efficiency ($Y_{star} > 0.5$), particularly at high redshift (see Fig. 4). The effect of this cooling excess is to sink more gas in the core to maintain the pressure support, thus making the overall baryon fraction supercosmic and the gas fraction less concentrated at high redshift. At R_{500} and R_{200}, the dispersion in the estimate of Y_b is 2–3 per cent of the measured mean (Fig. 3). We explain the reduction in the scatter at large radii by the common history that the baryons experience in our simulations when the properties are averaged over a volume

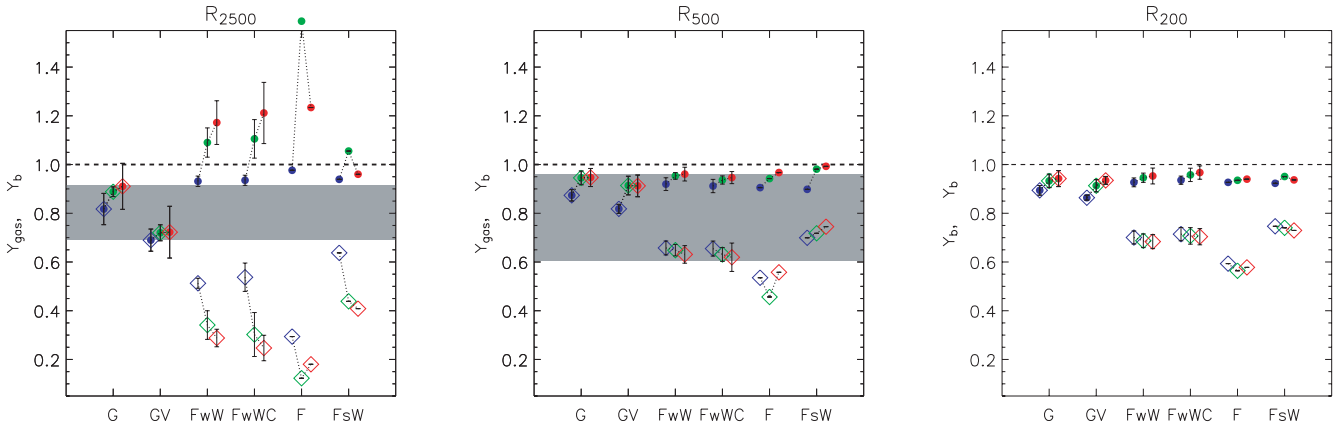

Figure 3. The gas (open diamonds) and total baryon (full circles) mass fractions, in units of the cosmic baryonic value at R_{2500} (left panel), R_{500} (central panel) and R_{200} (right panel). For each physical case considered, we plot the mean and standard deviation values measured at $z = 0$, 0.7 and 1. The shaded region shows the error-weighted mean and standard deviation of (1) $f_{\rm gas}(R_{2500})$ estimated from 26 X-ray-luminous galaxy clusters in Allen et al. (2004, quoted in their table 2 for an LCDM universe), and (2) $f_{\rm gas}(R_{500})$ from 35 highly luminous ($L_{\rm X} \gtrsim 10^{45}$ erg s^{-1}) objects in Ettori & Fabian (1999). The observational data are normalized to $\Omega_{\rm b}h^2 = 0.0214 \pm 0.0020$ (Kirkman et al. 2003), $H_0 = 70$ km s^{-1} Mpc^{-1} and $\Omega_{\rm m} = 0.3$.

large enough not to be dominated by the physics of the core. With respect to the mean values measured at R_{2500}, $Y_{\rm star}$ decreases by a factor of $\gtrsim 2$ and $Y_{\rm gas}$ increases by more than 30 per cent, with peaks of 2–3 when no winds, or weak winds combined with the effect of conduction, affect the ICM physics (Fig. 5). The ratio $f_{\rm gas}/f_{\rm star}$, which is $\lesssim 1$ at R_{2500} and $z \gtrsim 0.3$, increases with both radius and redshift and becomes $\simeq 3$ at R_{200} and $z = 0$ in the presence of winds (see Fig. 5). Once again, the absence of galactic winds increases the efficiency of star formation and leaves the $f_{\rm gas}/f_{\rm star}$ ratio below 2 within the virial radius. These values are well above the observed constraints, also plotted in Fig. 5. Lin, Mohr & Stanford (2003) compare the gas mass measured in nearby X-ray-bright galaxy clusters with the stellar masses evaluated from K-band luminosities of the member galaxies. From their estimates, converted to the total mass measurements in Arnaud, Pointecouteau & Pratt (2005), we infer an average $M_{\rm gas}/M_{\rm star} \approx 8.7$ (rms = 2.7) at R_{500} in systems with gas temperatures larger than 3 keV, which is still a factor of between 2.5 and 6 larger than that obtained in our simulated objects (Fig. 5), thus witnessing the presence of significant overcooling.

4 COMPARISON TO PREVIOUS ANALYSES

While the comparison between the results of different non-radiative simulations is relatively straightforward, when extra physics is included, such as radiative cooling, star formation and stellar feedback, the results on the hot and cool baryon distributions are sensitive to the scheme implemented. Therefore, this difference has to be taken into account in performing such a comparison.

In their non-radiative simulations, Eke et al. (1998) found that the gas fraction within $R_{\rm vir}$ is, on average, 87 per cent of the cosmic value, which is reached at about 3 $R_{\rm vir}$. For dynamically relaxed systems, they measure $Y_{\rm gas} = 0.824 \pm 0.033$ at $r = 0.25\,R_{\rm vir} \approx R_{2500}$ (as quoted in Allen et al. 2004). No evident evolution is present between $z = 1$ and 0. A comparable value was obtained as the average of the baryon fraction measured in a set of non-radiative simulations of one single cluster presented in the Santa Barbara comparison project (Frenk et al. 1999), with $f_{\rm b}/(\Omega_{\rm b}/\Omega_{\rm m})$ of 0.92 (rms = 0.07) at the virial radius. Similar results have also been obtained in other SPH simulations (e.g. Bialek et al. 2001; Muanwong et al. 2002).

These results agree with our estimates for our simulations of massive galaxy clusters with gravitational heating only: $Y_{\rm b}(<R_{200}) = 0.89 \pm 0.02$ (0.90 ± 0.03 at $R_{\rm vir}$). A slight increase at high redshift is however measured ($Y_{\rm b} = 0.94 \pm 0.03$ at $z = 1$). On the contrary, the baryon fraction decreases moving inwards, with $Y_{\rm b}(<R_{500}) = 0.87$ and $Y_{\rm b}(<R_{2500}) = 0.82$.

Kravtsov et al. (2005) studied the baryon fraction in nine galaxy clusters spanning a decade in mass and simulated with the Eulerian adaptive mesh refinement N-body + gas dynamics ART code, for both non-radiative and radiative cases. For non-radiative simulations, they measure $Y_{\rm b} \approx 1$ (at $r \gtrsim 3\,R_{\rm vir}$), 0.97 ± 0.03 (at $R_{\rm vir}$), 0.94 ± 0.03 (at R_{500}) and 0.85 ± 0.08 (at R_{2500}), which are consistently higher than our values by a few per cent. This systematic difference by $\approx$5 per cent at $r \gtrsim R_{2500}$ has already been shown by the comparison between the ART and GADGET codes discussed in Kravtsov et al. (2005). Even though it is smaller than the 10 per cent differences measured in the Santa Barbara cluster comparison project (Frenk et al. 1999) between the gas fraction obtained from Eulerian and SPH codes, it is still relevant when using simulations to calibrate systematics in the estimate of the baryon fraction in clusters.

When radiative cooling and other physical processes are turned on, the number of reliable comparisons that can be done is reduced. In the radiative simulations of Muanwong et al. (2002), $Y_{\rm gas}$ is between 0.6 and 0.7 in high-M systems and $Y_{\rm b} \approx 0.9$ at the virial radius. When preheating with an extra energy of 1.5 keV per particle at $z = 4$, these authors find $Y_{\rm gas} \sim Y_{\rm b} \approx 0.8$–0.9. Kravtsov et al. (2005) measure the gas fraction to rise from 0.46 ± 0.06 (at R_{2500}) to 0.65 ± 0.06 (at $R_{\rm vir}$), whereas $Y_{\rm b}$ always remains around 1 (from 1.22 ± 0.11 at R_{2500} to 1.02 ± 0.02 at $R_{\rm vir}$). These values are roughly in agreement with our results, in particular for the set of simulated objects with weak winds: at $z = 0$, $Y_{\rm gas} = 0.51 \pm 0.02$ at R_{2500} and 0.70 ± 0.03 at R_{200}, while $Y_{\rm b}$ is flat around 0.93 ± 0.02 and never supercosmic, i.e. $Y_{\rm b} < 1$. Different numerical implementations of the cooling, star formation and feedback processes are expected to contribute to this systematic difference between the predictions of ART and GADGET simulations. These differences are, in fact, more significant in the radiative runs and depend on the amount of baryons cooled in stars (see also Kravtsov et al. 2005). Such differences, which are numerical in origin, should definitely be considered as theoretical uncertainties, when using simulations to calibrate systematic biases in the observational estimate of the baryon fraction within clusters. The action of stronger winds is to increase the gas fraction, whereas the absence of winds reduces $Y_{\rm gas}$ to 0.29 and 0.59 at R_{2500} and R_{200}, respectively.

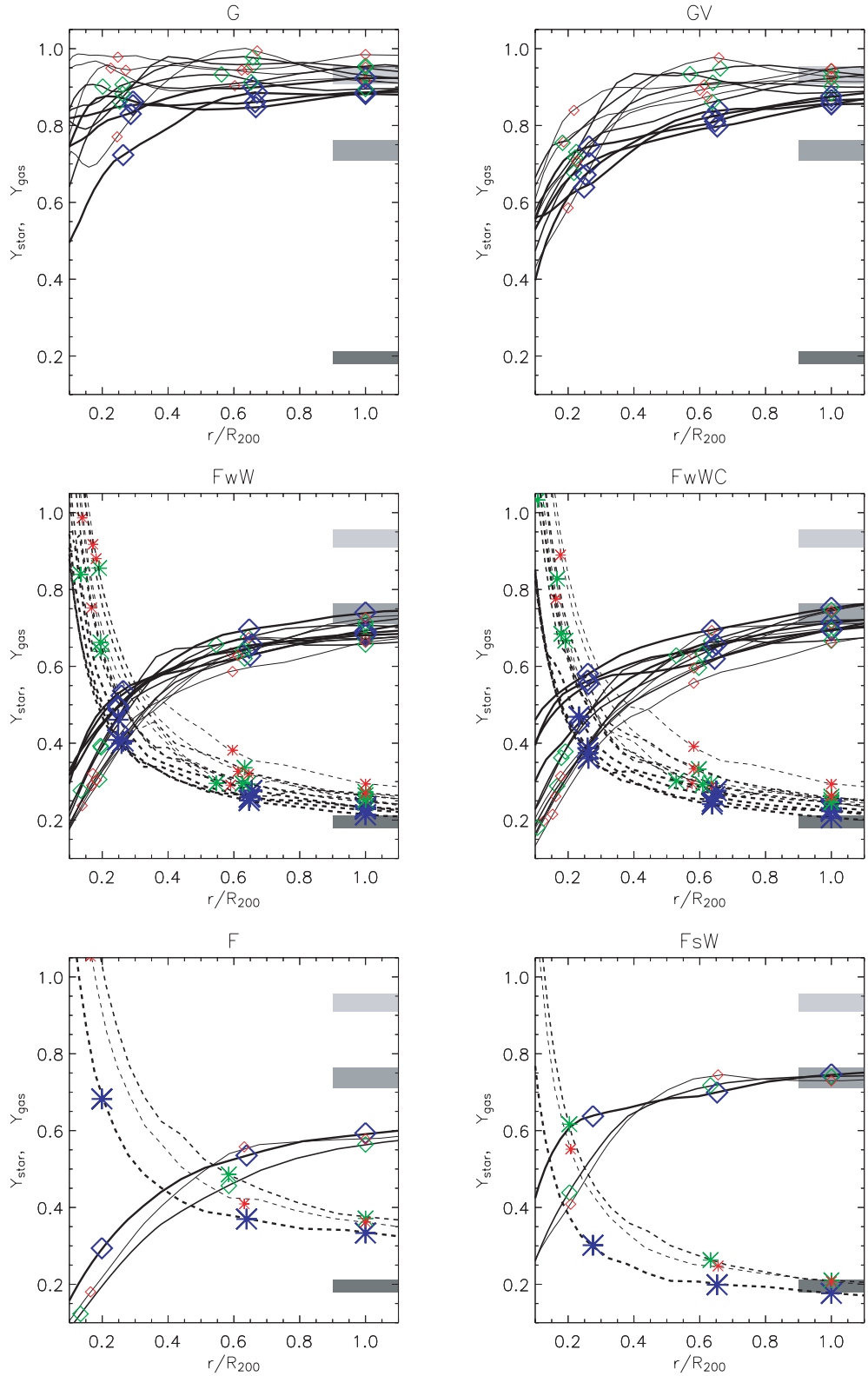

Figure 4. Comparison between the outputs of the six different physical schemes investigated. The gas (solid line) and stellar (dashed line) mass fractions, normalized to the cosmic value, are plotted at R_{2500} ($\approx$0.3 R_{200}), R_{500} ($\approx$0.7 R_{200}) and R_{200}. Their evolution with redshift is indicated by the thickness of the lines (lines/symbols from thick/large to thin/small: $z = 0$, 0.7, 1). The shaded regions indicate the 1 σ range of Y_{star}, Y_{gas} and Y_b measured at R_{200} and $z = 0$ for the cluster set extracted from the cosmological box.

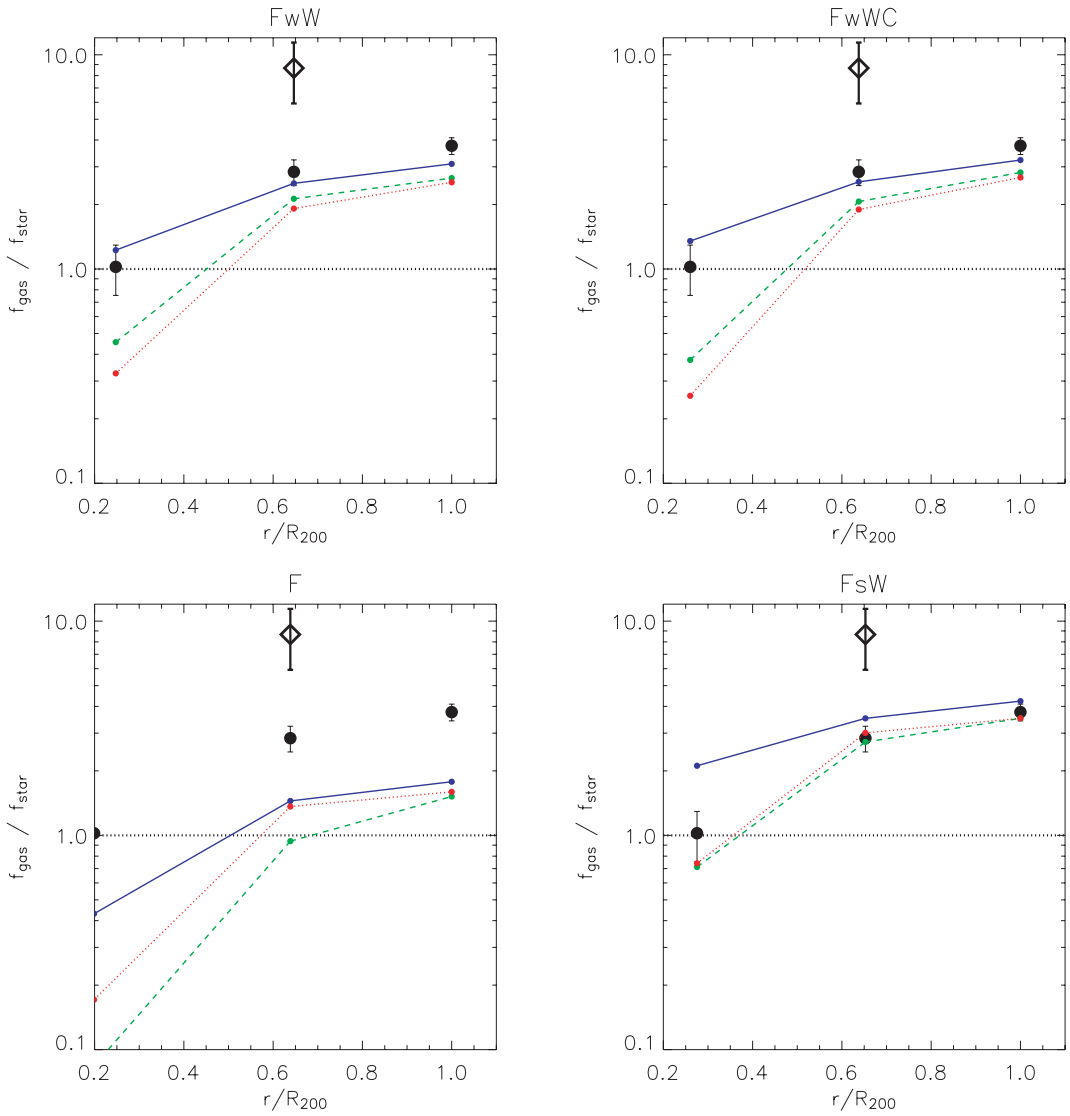

Figure 5. Ratios between the cumulative gas and stellar mass fractions within a given radius as a function of redshift (solid line, $z = 0$; dashed line, $z = 0.7$; dotted line, $z = 1$) for the different physics included in the simulations. The large full circles show the mean value (and relative standard deviation) obtained from the cosmological sample. The open diamonds indicate the ratios expected, for a given M_{500}, from equation (10) of Lin et al. (2003), based on near-infrared observations of massive X-ray galaxy clusters.

5 IMPLICATIONS FOR THE CONSTRAINTS ON COSMOLOGICAL PARAMETERS

Our results have a direct implication on the systematics that affect the constraints on the cosmological parameters obtained through the cluster baryon mass fraction (e.g. White et al. 1993; Evrard 1997; Allen et al. 2002; Ettori et al. 2003; Ettori 2003; Allen et al. 2004). We recall that, once a representative gas fraction, denoted here $\hat{f}_{\rm gas}$, is directly measured from X-ray observations and a statistical relation between the average $\hat{f}_{\rm star}$ and $\hat{f}_{\rm gas}$ is adopted, the cosmic mass density parameter can then be evaluated as

$$\Omega_{\rm m} = \frac{Y_{\rm b}\Omega_{\rm b}}{\hat{f}_{\rm gas}(1 + \hat{f}_{\rm star}/\hat{f}_{\rm gas})}, \qquad (1)$$

where the 'hat' indicates the observed quantities and the cosmic baryon density $\Omega_{\rm b}$ is assumed from primordial nucleosynthesis calculations or the measured anisotropies in the cosmic microwave background. In recent years this method has also been extended to measure the dark energy density parameters (Ω_Λ, w; see e.g. Allen et al. 2002, 2004; Ettori et al. 2003) under the assumption that the gas fraction remains constant in redshift (Sasaki 1996; Pen 1997). Since the gas fraction scales with the angular diameter distance as $f_{\rm gas} \propto d_{\rm A}^{1.5}$, the best choice of cosmological parameters is defined as the set of values that minimizes the χ^2 distribution of the measured gas fraction at different redshifts with respect to the reference value:

$$f_{\rm gas}^{\Lambda{\rm CDM}} = \frac{Y_{\rm b}\Omega_{\rm b}\Omega_{\rm m}^{-1}}{(1 + \hat{f}_{\rm star}/\hat{f}_{\rm gas})} \left[\frac{d_{\rm A}(z; \Omega_{\rm m} = 0.3; \Omega_\Lambda = 0.7)}{d_{\rm A}(z; \Omega_{\rm m}; \Omega_\Lambda)}\right]^{1.5}. \qquad (2)$$

Despite its conceptual simplicity and straightforward application, this method makes some assumptions that have to be tested before the error bars estimated for the matter and dark energy density parameters can be accepted as robust and reliable determinations of both statistical and systematic uncertainties. In the present discussion, we highlight two of the assumptions generally adopted, but never verified: (1) the mean value of $Y_{\rm b}$ does not evolve with

redshift; and (2) a fixed ratio between $f_{\rm star}$ and $f_{\rm gas}$ holds in a cluster at any radius and redshift. As we have shown here, neither of these two assumptions is valid in our simulated data set whatever physics is included in the simulations, in particular when considering the inner part of the clusters. Allen et al. (2004) use the simulation results by Eke et al. (1998) to fix $Y_{\rm b} = 0.824 \pm 0.033$ at $r \approx R_{2500}$ for their sample of *Chandra* exposures of the largest relaxed clusters with redshift between 0.07 and 0.9. We notice, for instance, that, while this value is in agreement with our simulation results at $z = 0$ in the runs with gravitational heating only ($Y_{\rm b} = 0.82 \pm 0.06$), it is definitely lower than what we estimate at higher redshift (e.g. $Y_{\rm b} = 0.86, 0.89, 0.91$ at $z = 0.3, 0.7, 1$, respectively). This increase of $Y_{\rm b}$ with redshift is the consequence of the different accretion pattern of shock-heated baryons at different epochs. At later times, accreting gas has had more time to be pre-shocked into filaments. As a consequence, they have a relatively higher entropy, thus relatively increasing the radius (in units of the virial radius) where accretion shocks take place. This is the reason why, as shown in Fig. 2, at $z = 1$, $f_{\rm b}$ reaches the cosmic value at relatively smaller radii than at $z = 0$.

Since the tighter cosmological constraints provided by the cluster gas fraction alone are on $\Omega_{\rm m}$ (of the order of 16 per cent at 1σ level; e.g. Allen et al. 2004), we try to quantify the effect on this estimate of the variation of the baryonic components with radius and redshift. To this purpose, we use equation (1) and evaluate first how $\Omega_{\rm m}$ changes on varying $Y_{\rm b}$. The increasing baryon fraction with redshift induces a larger estimate of $\Omega_{\rm m}$ with respect to that obtained from local measurements of $Y_{\rm b}$:

$$\frac{\Omega'_{\rm m} - \Omega_{\rm m}}{\Omega_{\rm m}} = \frac{\Delta\Omega_{\rm m}}{\Omega_{\rm m}} = \frac{Y_{\rm b}(<R_\Delta, z = z_0)}{Y_{\rm b}(<R_\Delta, z = 0)} - 1 \qquad (3)$$

is $+0.09$ at $R_\Delta = R_{2500}$ and $z_0 = 0.7$ for the case with gravitational heating only and $+0.11$ at $z_0 = 1$. (Here the prime indicates the corrected value with respect to the reference one.) Using instead the runs with reduced viscosity, the deviation decreases to about $+0.05$. As for the radiative runs, the bias is of the order of 20 per cent, which reduces to 2 per cent in the presence of strong winds at $z = 1$. When outer cluster regions are mapped (i.e. $r \sim R_{500}$), the deviation converges to similar amounts due to the limited impact of cooling and feedback over large volumes: variations between $+0.03$ (weak winds) and $+0.10$ (strong winds) become comparable to $\Delta\Omega_{\rm m}/\Omega_{\rm m} \approx +0.08$ as measured in non-radiative runs.

A further contribution to the uncertainties comes from the dependence upon the radius and redshift of the ratio $f_{\rm star}/f_{\rm gas}$. In the observational determination of the baryon fraction from equation (1), this quantity is generally assumed to be 0.16, as measured in the Coma cluster within the virial radius [e.g. White et al. (1993); note that our estimate from Lin et al. (2003) and adopting the total mass measurements in Arnaud et al. (2005) is 0.11 ± 0.04]. If we compare the ratio $\phi = f_{\rm star}/f_{\rm gas}$ measured for a Coma-like simulated cluster at R_{200} and $z = 0$ with the estimates at other redshifts ($z_0 = 0.7$ and 1; see e.g. Fig. 5), we evaluate from equation (1)

$$\frac{\Omega'_{\rm m} - \Omega_{\rm m}}{\Omega_{\rm m}} = \frac{\Delta\Omega_{\rm m}}{\Omega_{\rm m}} = \frac{1 + \phi(<R_\Delta, z = 0)}{1 + \phi(<R_\Delta, z = z_0)} - 1 \approx -0.05. \qquad (4)$$

When $\phi = f_{\rm star}/f_{\rm gas}$ measured locally at R_{2500} is compared with the corresponding value at different redshifts, the deviation ranges between -0.74 (when winds are excluded) and -0.38 (when strong winds are present), whereas it is about -0.10 at R_{500}.

As for the runs with gravitational heating only, the effect of the variation of $Y_{\rm b}$ with redshift and overdensity implies that $\Delta\Omega_{\rm m}/\Omega_{\rm m} \lesssim +0.11$, thus comparable to the current statistical uncertainties from *Chandra* observations of the massive clusters out to $z = 1.3$ (Ettori et al. 2003; Allen et al. 2004). However, when the extra physics of the radiative runs is included, $\Delta\Omega_{\rm m}/\Omega_{\rm m}$ has two contributions of $\approx +0.10$ and $\lesssim -0.05$, due to an increase with redshift of (1) $Y_{\rm b}$ (see Fig. 3) and (2) the stellar to gas mass fraction ratio (see Fig. 5). Both these effects are caused by more efficient star formation in high-redshift clusters.

In general, our results indicate that it may be dangerous to use simulations to calibrate observational biases for precise determination of cosmological parameters from the gas fraction in clusters. Although none of our simulation models includes a fair description of the actual ICM physics, it is interesting that different models provide different redshift-dependent corrections for the estimate of the cosmic baryon fraction from observations of the gas and star density distribution within clusters. If applied to observational data, such corrections would induce sizeable differences in the determination of the matter and dark energy density parameters.

6 SUMMARY AND DISCUSSION

We have analysed the distribution of gas and stellar mass fraction in simulated massive X-ray galaxy clusters as a function of (i) the radius expressed in the form of R_{2500}, R_{500} and R_{200}, (ii) the redshift at which the structure is identified, and (iii) the physical processes determining the evolution of the baryons in the cluster potential wells (i.e. gravitational heating, radiative cooling, star formation, conduction and galactic winds powered by supernova explosions).

Our main results can be summarized as follows:

(i) As for the cluster set extracted from a cosmological box, which are simulated by including cooling, star formation and feedback with weak ($340\,{\rm km\,s^{-1}}$) winds, at R_{200} we find $Y_{\rm b} = 0.93$, $Y_{\rm gas} = 0.74$ and $Y_{\rm star} = 0.20$, with scatter around these values of 2, 4 and 8 per cent, respectively. These results are virtually independent of cluster mass over the range $M_{\rm vir} \approx (0.5\text{–}13) \times 10^{14}\, h^{-1}\, {\rm M}_\odot$. The dispersion relative to the mean value measured at R_{2500} is a factor of about 3 larger than at R_{200}.

(ii) In the four massive ($M_{200} > 10^{15}\, h^{-1}\, {\rm M}_\odot$) galaxy clusters simulated with six different physical schemes, we find that the cosmic value of the baryon fraction $\Omega_{\rm b}/\Omega_{\rm m}$ is reached at about $3\, R_{200}$. At $z = 0$ the gas fraction increases radially, reaching 50 (80) per cent of the value measured at R_{200} at $r \approx 0.1(0.3)\, R_{200}$. At $z = 1$ the same values are reached at radii that are about 40 per cent larger. This indicates that $f_{\rm gas}$ tends to be less concentrated at higher redshift, where more efficient star formation causes a more efficient removal of gas from the hot phase in the central cluster regions. We also find that in these clusters the amount of hot baryons, in units of the cosmic value, is less scattered and less dependent on the particular physics adopted when it is measured over larger cluster regions. At $z = 0$ in the runs with gravitational heating only, $Y_{\rm b} = f_{\rm bar}/(\Omega_{\rm b}/\Omega_{\rm m})$ ranges between 0.82 ± 0.06 (at R_{2500}) and 0.89 ± 0.02 (at R_{200}). At $z = 1$ it increases to 0.91 ± 0.10, 0.95 ± 0.04 and 0.94 ± 0.03 at R_{2500}, R_{500} and R_{200}, respectively. This increase of $Y_{\rm b}$ with z is due to the smaller radii (in units of the virial radius) at higher redshift where shock-heated baryons accrete, permitting the $f_{\rm b}$ values to reach the cosmic value at higher overdensities, for example, at $z = 1$ rather than at $z = 0$ (see e.g. Fig. 2). These values are roughly in agreement with observational constraints obtained from highly X-ray-luminous clusters (e.g. Ettori & Fabian 1999; Allen et al. 2004) at R_{2500} and R_{500}. Using an SPH scheme with reduced viscosity, the non-thermal pressure support contributed by turbulent

gas motions reduces the gas fraction by 15 per cent at R_{2500} and by $\sim$5 per cent at $r > R_{500}$.

Adding extra physics to the action of gravity reduces the amount of diffuse baryons by 20–40 (20–65) per cent at R_{500} (R_{2500}). This is due to the high star formation efficiency, which is not sufficiently mitigated by our assumed supernova feedback. The presence of strong winds (here it is assumed that $v \lesssim 480\,\mathrm{km\,s^{-1}}$) induces the following effects: (1) a reduction of $Y_{\rm star}$ by about a factor of 2 with respect to the case with no winds; (2) a milder radial dependence of $Y_{\rm star}$ and $Y_{\rm gas}$; and (3) larger values for the ratio between $f_{\rm gas}$ and $f_{\rm star}$, which however is still smaller, by about a factor of 2.5, than the observed values (Lin et al. 2003).

(iii) At R_{2500}, the estimate of $Y_{\rm b}$ is strongly affected by the physics included in the simulations. Supercosmic values are found for the radiative runs, as a consequence of the exceedingly efficient cooling process, which causes a rapid sinking of baryons in the cluster cores. Moreover, differences in the formation history of individual clusters contribute to a wider spread in the $Y_{\rm b}$ values, as shown in the runs including only gravitational heating. In these cases, the standard deviation is about 10 per cent.

(iv) At R_{500} and R_{200}, the dispersion in the estimate of $Y_{\rm b}$ is 2–3 per cent of the measured mean. With respect to the mean values measured at R_{2500}, $Y_{\rm star}$ decreases by a factor of $\gtrsim$2 and $Y_{\rm gas}$ increases by more than 1.3, with peaks of 2–3 in the simulations without winds, or with weak winds combined with conduction at one-third the Spitzer value.

We explain the reduction in the scatter at $r > R_{500}$ by the common history that the baryons experience when their properties are averaged over a large enough volume. In the outer regions, gas evolution is mainly driven by the action of gravity. The ratio $f_{\rm gas}/f_{\rm star}$, which is $\lesssim$1 at R_{2500} and $z \gtrsim 0.3$, increases with radius and redshift and becomes $\simeq$3 at R_{200} and $z = 0$ in the presence of winds.

(v) Our results have direct implications on the calibration of the systematic effects that limit the use of the X-ray gas mass fraction as a cosmological tool (e.g. Evrard 1997; Ettori et al. 2003; Allen et al. 2004). Owing to the uncertainties in the modelling of the ICM, we emphasize that our simulations cannot be used to calibrate the observed $f_{\rm gas}$. However, our results emphasize the potential problems related to estimating the cosmic baryon fraction from the gas mass fraction as measured in central cluster regions, i.e. the variation of $Y_{\rm b}$ with redshift and a proper estimate of the contribution of stars in galaxies to the total cluster baryon budget as a function of radius and redshift.

For the non-radiative runs the effect of the variation of $Y_{\rm b}$ with redshift and overdensity implies $\Delta\Omega_{\rm m}/\Omega_{\rm m} \lesssim +0.11$, which is comparable to the typical statistical uncertainties from *Chandra* observations of massive clusters out to redshift $z = 1.3$ (Ettori et al. 2003; Allen et al. 2004). However, when star formation and feedback are also included, $\Delta\Omega_{\rm m}/\Omega_{\rm m}$ has two contributions of $\approx +0.10$ and $\lesssim -0.05$, due to an increase with redshift of (1) $Y_{\rm b}$ (see Fig. 3) and (2) the ratio between stellar and gas mass (see Fig. 5).

Our results show that star formation in our radiative runs is still too efficient, especially in the cluster central regions, even in the presence of rather strong galactic winds. As a result, the impact of cooling and star formation in the simulated clusters is still much larger than in realistic cases. On the one hand, this calls for the need to introduce more effective feedback mechanisms, e.g. related to active galactic nuclei (AGN), which are able to prevent overcooling in the central cluster regions [see, for example, the effect of the injection of supersonic AGN jets in the ICM of simulated clusters in Zanni et al. (2005)]. On the other hand, our analysis demonstrates that using simulations to calibrate the systematic uncertainties in the estimate of cosmological parameters from the cluster gas mass fraction may be quite problematic, especially if it has to be used as a high-precision tool to measure the cosmic density parameters associated with matter and dark energy.

ACKNOWLEDGMENTS

The simulations have been performed using: the IBM-SP4 machine at the 'Consorzio Interuniversitario del Nord-Est per il Calcolo Elettronico' (CINECA, Bologna), with CPU time assigned thanks to the INAF–CINECA grant; the IBM-SP3 machine at the Italian Centre of Excellence 'Science and Applications of Advanced Computational Paradigms', Padova; and the IBM-SP4 machine at the 'Rechenzentrum der Max-Planck-Gesellschaft' at the 'Max-Planck-Institut für Plasmaphysik', with CPU time assigned to the 'Max-Planck-Institut für Astrophysik'. This work has been partially supported by the INFN–PD51 grant and by MIUR. The anonymous referee is thanked for insightful comments.

REFERENCES

Allen S. W., Schmidt R. W., Fabian A. C., 2002, MNRAS, 334, L11
Allen S. W., Schmidt R. W., Ebeling H., Fabian A. C., van Speybroeck L., 2004, MNRAS, 353, 457
Arnaud M., Pointecouteau E., Pratt G. W., 2005, A&A, 441, 893
Bialek J. J., Evrard A. E., Mohr J. J., 2001, ApJ, 555, 597
Borgani S. et al., 2004, MNRAS, 348, 1078
Dolag K., Jubelgas M., Springel V., Borgani S., Rasia E., 2004, ApJ, 606, L97
Dolag K., Vazza F., Brunetti G., Tormen G., 2005, MNRAS, 364, 753
Eke V. R., Navarro J. F., Frenk C. S., 1998, ApJ, 503, 569
Ettori S., 2003, MNRAS, 344, L13
Ettori S., Fabian A. C., 1999, MNRAS, 305, 834
Ettori S., Tozzi P., Rosati P., 2003, A&A, 398, 879
Ettori S. et al., 2004, MNRAS, 354, 111
Evrard A. E., 1990, ApJ, 363, 349
Evrard A. E., 1997, MNRAS, 292, 289
Evrard A. E., Henry J. P., 1991, ApJ, 383, 95
Frenk C. et al., 1999, ApJ, 525, 554
Jubelgas M., Springel V., Dolag K., 2004, MNRAS, 351, 423
Kaiser N., 1991, ApJ, 383, 104
Kay S. T., Thomas P. A., Jenkins A., Pearce F. R., 2004, MNRAS, 355, 1091
Kirkman D., Tytler D., Suzuki N., O'Meara J. M., Lubin D., 2003, ApJS, 149, 1
Kravtsov A. V., Nagai D., Vikhlinin A. A., 2005, ApJ, 625, 588
Lin Y. T., Mohr J. J., Stanford S. A., 2003, ApJ, 591, 749
Lubin L. M., Cen R., Bahcall N. A., Ostriker J. P., 1996, ApJ, 460, 10
Mathiesen B. F., Evrard A. E., 2001, ApJ, 546, 100
Mazzotta P., Rasia E., Moscardini L., Tormen G., 2004, MNRAS, 354, 10
Metzler C. A., Evrard A. E., 1994, ApJ, 437, 564
Mohr J. J., Mathiesen B., Evrard A. E., 1999, ApJ, 517, 627
Morris J. P., Monaghan J. J., 1997, J. Comput. Phys., 136, 41
Muanwong O., Thomas P. A., Kay S. T., Pearce F. R., 2002, MNRAS, 336, 527
Murante G. et al., 2004, ApJ, 607, L83
Navarro J. F., Frenk C. S., White S. D. M., 1995, MNRAS, 275, 720
Pen U.-L., 1997, New Astron., 2, 309
Rasia E. et al. 2005, MNRAS, submitted
Roussel H., Sadat R., Blanchard A., 2000, A&A, 361, 429
Sasaki S., 1996, PASJ, 48, L119
Springel V., 2005, MNRAS, 364, 1105
Springel V., Hernquist L., 2002, MNRAS, 333, 649
Springel V., Hernquist L., 2003, MNRAS, 339, 289
Springel V., Yoshida N., White S. D. M., 2001, New Astron., 6, 79
Tormen G., 1997, MNRAS, 290, 411

Vikhlinin A., 2005, ApJ, submitted (astro-ph/0504098)
White S. D. M., 1996, in Schaeffer R., Silk J., Spiro M., Zinn-Justin J., eds, Cosmology and Large-Scale Structure. Elsevier Scientific, Amsterdam, p. 349
White S. D. M., Navarro J. F., Evrard A. E., Frenk C. S., 1993, Nat, 366, 429
Yoshida N., Sheth R. K., Diaferio A., 2001, MNRAS, 328, 669
Zanni C., Murante G., Bodo G., Massaglia S., Rossi P., Ferrari A., 2005, A&A, 429, 399

This paper has been typeset from a TEX/LATEX file prepared by the author.